Supplemental Document

Biomedical Optics EXPRESS

High-throughput line-illumination Raman microscopy with multislit detection: supplement

KENTARO MOCHIZUKI,[1,2,10] YASUAKI KUMAMOTO,[1,3,10] SHUNSUKE MAEDA,[1] MASATO TANUMA,[4] ATSUSHI KASAI,[4] MASASHI TAKEMURA,[2] YOSHINORI HARADA,[2] HITOSHI HASHIMOTO,[3,4,5,6,7] HIDEO TANAKA,[2] NICHOLAS ISAAC SMITH,[3,8] AND KATSUMASA FUJITA[1,2,3,9,*]

[1]*Department of Applied Physics, Osaka University, Suita, Osaka 565-0871, Japan*
[2]*Department of Pathology and Cell Regulation, Kyoto Prefectural University of Medicine, Kamigyo-ku, Kyoto 602-8566, Japan*
[3]*Institute for Open and Transdisciplinary Research Initiatives, Osaka University, Suita, Osaka 565-0871, Japan*
[4]*Laboratory of Molecular Neuropharmacology, Graduate School of Pharmaceutical Sciences, Osaka University, Suita, Osaka 565-0871, Japan*
[5]*Molecular Research Center for Children's Mental Development, United Graduate School of Child Development, Osaka University, Kanazawa University, Hamamatsu University School of Medicine, Chiba University and University of Fukui, Suita, Osaka 565-0871, Japan*
[6]*Institute for Datability Science, Osaka University, Suita, Osaka 565-0871, Japan*
[7]*Department of Molecular Pharmaceutical Sciences, Graduate School of Medicine, Osaka University, Suita, Osaka 565-0871, Japan*
[8]*Biophotonics Laboratory, Immunology Frontier Research Center, Osaka University, Suita, Osaka 565-0871, Japan*
[9]*Advanced Photonics and Biosensing Open Innovation Laboratory, AIST-Osaka University, Osaka University, Suita, Osaka 565-0871, Japan*
[10]*These authors contributed equally*
[*]*fujita@ap.eng.osaka-u.ac.jp*

Supplement DOI: https://doi.org/10.6084/m9.figshare.21806352

Parent Article DOI: https://doi.org/10.1364/BOE.480611

High-throughput line-illumination Raman microscopy with multislit detection: Supplement 1

1. Concept

Image acquisition time T is generally expressed by the total signal accumulation time T_A and the total detector readout time T_R as follows.

$$T = T_A + T_R \quad \text{(eq. 1)}$$

In a conventional laser scanning Raman microscopy using a focused laser beam spot to scan a sample two dimensionally (Fig. S1A), $T_{A,spot}$ and $T_{R,spot}$ are expanded as the following equations,

$$T_{A,spot} = T_a \times (N_x \times N_y) \quad \text{(eq. 2)},$$

$$T_{R,spot} = T_r \times (N_x \times N_y) \quad \text{(eq. 3)},$$

where T_a and T_r are the signal accumulation time and detector readout time for each spectrum acquisition, respectively, and N_x and N_y are the numbers of image pixels in x and y, respectively. According to the equations 2 and 3, both the signal accumulation time and the detector readout time increase as the image resolution $N_x \times N_y$ increases and therefore effective acceleration of Raman imaging is implemented by reducing their values.

Slit-scanning Raman microscopy, which is an established fast Raman hyperspectral microscopy using spontaneous Raman scattering, can be viewed as the precursor of the new technique presented here (Fig. S1B). The entrance slit of a spectrophotometer is used for scanning; the sample region imaged at the slit via an imaging system is measured with the spectrophotometer equipped with a camera (having N_y and N_λ pixels in the directions parallel and perpendicular to the slit respectively) and a one-dimensional Raman spectral image with N_y image pixels and N_λ wavenumber pixels is acquired. After the acquisition, the sample region is shifted to the direction perpendicular to the slit by a constant distance. These sequential steps are continued N_X times and consequently a two-dimensional Raman hyperspectral image with $N_x \times N_y$ image pixels is acquired. In this procedure, $T_{A,slit}$ and $T_{R,slit}$ result in the following equations 4 and 5, respectively.

$$T_{A,slit} = T_a \times N_x = T_{A,spot} / N_y \quad \text{(eq. 4)}$$

$$T_{R,slit} = T_r \times N_y \times N_x = T_{R,spot} \quad \text{(eq. 5)}$$

The signal accumulation time T_A in slit-scanning Raman microscopy is reduced by N_y in comparison to conventional laser-scanning Raman microscopy. This is because the signal acquisition number is reduced from $N_x \times N_y$ to N_x while the unit signal accumulation time is kept. The signal readout time T_R, on the other hand, does not change because the unit detector readout time T_r and the total number of spectra acquired $N_y \times N_x$ are kept.

The presented new technique, multiline-illumination Raman microscopy (Fig. S1C), has a similar working principle to that of slit-scanning Raman microscopy but uses custom multiple slits (N_{MS} slits arranged in a constant spacing orthogonally to the direction of the slit) that are installed at the spectrophotometer entrance**,** instead of the conventional single slit. In multiline-illumination Raman microscopy, $N_y \times N_{MS}$ spectra are acquired with a single acquisition and the number of acquisition is reduced to N_x / N_{MS}, in comparison to the single

slit case. Consequently, the signal accumulation time $T_{A,multi}$ for taking an $N_x \times N_y$ Raman hyperspectral image is expressed by equation 6.

$$T_{A,multi} = T_a \times (N_x / N_{MS}) = T_{A,slit} / N_{MS} \quad \text{(eq. 6)}$$

In practice, the effective detector readout time for each spectrum acquisition also can be shortened because the number of sensors of the spectrophotometer camera is limited, *i.e.*, $N_y \times N_\lambda$; to acquire $N_y \times N_{MS}$ spectra by a camera with having $N_y \times N_\lambda$ sensors, only N_λ / N_{MS} sensors are used for recording a Raman spectrum and hence, the unit detector readout time is reduced by N_{MS}. Consequently, the detector readout time $T_{R,multi}$ for taking an $N_x \times N_y$ Raman hyperspectral image is expressed by equation 7.

$$T_{R,multi} = (T_r / N_{MS}) \times N_y \times N_x = T_{R,slit} / N_{MS} \quad \text{(eq. 7)}$$

Overall, multiline-illumination Raman microscopy accelerates Raman hyperspectral imaging by N_{MS} times in comparison to slit-scanning Raman microscopy.

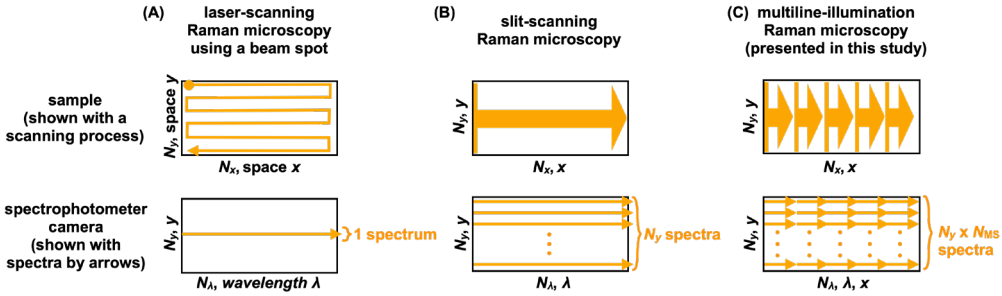

Fig. S1. Three types of laser-scanning Raman microscopy. (A) The focused laser beam spot is used for scanning two-dimensionally with $N_x \times N_y$ acquisitions. Each acquisition by a detector takes one spectrum. (B) Slit-scanning Raman microscopy needs one-dimensional scanning with N_x acquisitions. Each acquisition results in N_y spectra. The spectral number N_y is equivalent to the number of detector pixels in the direction of space y. (C) Multiline-illumination Raman microscopy conducts one-dimensional scanning with N_{MS} slits with N_x / N_{MS} acquisitions. Each acquisition results in $N_y \times N_{MS}$ spectra.

2. Guidance for selecting camera readout conditions

To determine the optimal readout rate for a measurement, one should consider the signal to noise ratio (SNR) and frame acquisition time of a measurement for different readout rates. SNR for a higher readout rate (Y_h) and a lower readout rate (Y_l) are expressed by the equations 8 and 9, respectively.

$$Y_\mathrm{h} = \frac{sE_\mathrm{h}}{\sqrt{(s+b+d)E_\mathrm{h}+{N_\mathrm{h}}^2}} \quad \text{(eq. 8)}$$

$$Y_\mathrm{l} = \frac{sE_\mathrm{l}}{\sqrt{(s+b+d)E_\mathrm{l}+{N_\mathrm{l}}^2}} \quad \text{(eq. 9)}$$

Here s, b, and d represent the signal counts, dark current, and background counts, respectively, for a unit time. E_h and E_l represent the signal accumulation times for the measurement with the higher and lower readout rates, respectively. N_h and N_l represent the readout noises for the higher and lower rates, respectively. The frame acquisition times for a higher readout rate (T_h) and a lower readout rate (T_l) are expressed by the equations 10 and 11, respectively.

$$T_\mathrm{h} = E_\mathrm{h} + R_\mathrm{h} \quad \text{(eq. 10)}$$

$$T_\mathrm{l} = E_\mathrm{l} + R_\mathrm{l} \quad \text{(eq. 11)}$$

Here R_h and R_l represent the frame readout times for the measurement with the higher and lower readout rates, respectively.

Now we consider the conditions where both SNR and imaging time are the same for different readout rates. By setting the equations of $Y_\mathrm{h} = Y_\mathrm{l}$ and $T_\mathrm{h} = T_\mathrm{l}$, the equation 12 is acquired.

$$s + b + d = \frac{{E_\mathrm{l}}^2{N_\mathrm{h}}^2-(E_\mathrm{l}+R_\mathrm{l}-R_\mathrm{h})^2{N_\mathrm{l}}^2}{E_\mathrm{l}(E_\mathrm{l}+R_\mathrm{l}-R_\mathrm{h})(R_\mathrm{l}-R_\mathrm{h})} \quad \text{(eq. 12)}$$

Equation 12 shows the condition under which the readout rate does not affect the measurement SNR at a given acquisition time. If the equation 12 is not satisfied, either a higher or lower readout rate will give a higher SNR. When the left side is less than the right side in equation 12, a slower readout provides a higher SNR. When the left side is greater than the right side in equation 12, a faster readout provides a higher SNR.

Selection of the readout rate does not just depend on the abovementioned guidance but does also depend on the purpose of a measurement, because the actual sum level of the signal and background is not constant in a measurement but is varied over a sample; samples contain both high-level and low-revel regions in signal and background. When the measurement purpose is to analyze a weak signal region with a high precision and accuracy, a slow readout rate that provides less readout is beneficial. This is likely the case for the bead measurement in Fig. 2, where the purpose was to confirm the optical performance of the developed microscope and the weak signal regions such as edge regions of single beads and the field near the image corners also needed to have a high SNR with a short imaging time. In contrast, a fast readout rate is beneficial when the measurement purpose is to quickly analyze the overall sample. This is often the case for the tissue measurements such as in Fig. 3.

The slow readout is also useful for samples that can be damaged by a large-dose laser irradiation. This is often the case for live cell measurements shown in Fig. 4.

3. Raman image reconstruction process and postprocess

MATLAB (Mathworks) was used for Raman image reconstruction. In the reconstruction process, a series of comb-like hyperspectral image data (such as the one shown in Fig. 2B) acquired by multiline illumination Raman microscopy was rearranged into a three-dimensional data cube of Space x × Space y × Wavelength λ. Because the Raman imaging data has a large background that can affect the subsequent data processing, a specific wavenumber range containing characteristic Raman bands of molecules of interest was extracted, and the minimal value was subtracted for each of the extracted spectra. Afterwards, singular value decomposition (SVD) was applied to the processed data cube and subsequently the loadings containing sample signals were used for data reconstruction. To minimize any influence of remaining background, we took a difference intensity at two different wavenumbers for reconstructing a Raman image of targeted molecules. Table S1 summarizes the detailed parameters for the reconstruction processes.

Table S1. Detailed parameters used for the Raman image reconstruction processes.

	PS/PMMA in Fig. 2	Kidney in Fig. 3		Liver in Fig. 3		Brain in Fig. 3	HeLa in Fig. 4
Wavenumber range (cm^{-1})	2922–3111	1442–1614	2806–2954	1530–1658	2798–2946	2822–2970	2806–2954
SVD loadings for image reconstruction	1st–6th	1st–5th	1st–4th	1st–4th	1st–6th	1st–4th	1st–4th
Band I Peak - bottom (cm^{-1})	2953–3096	1578–1610	2930–2862	1582–1650	2854–2830	2854–2830	2854–2830
Band II Peak - bottom (cm^{-1})	3051–3096	N/A	N/A	N/A	2930–2862	2930–2862	2930–2862

After the reconstruction process, postprocessing was applied to the reconstructed images. First, we corrected a stripe pattern that was generated due to the intensity discontinuity between two areas measured by adjacent two line illuminations. Briefly, each row of a reconstructed image was divided by the mean intensity projection of the image to the x axis (*i.e.* orthogonal to the line illumination) so that the stripe pattern was removed. In this process, the intensity distribution intrinsic to the sample was modified. To recover the intrinsic intensity distribution, the mean intensity projection was smoothed by a moving average filter with 51 pixel length and the derived smoothed signal was multiplied with the striped corrected image. Afterward, shading correction was applied as the reconstructed Raman images have weak signals at peripheral regions. Briefly, a reconstructed Raman image was divided by a rectangle image having an intensity distribution produced by a two-dimensional Gaussian function. The effects of stripe and shading corrections can be seen in Fig. S2.

Finally, the pseudo-color Raman images presented in the main text were formed on ImageJ 1.53e (National Institute of Health). The image brightness and contrast were adjusted for the visibilities of molecular distributions to be clear.

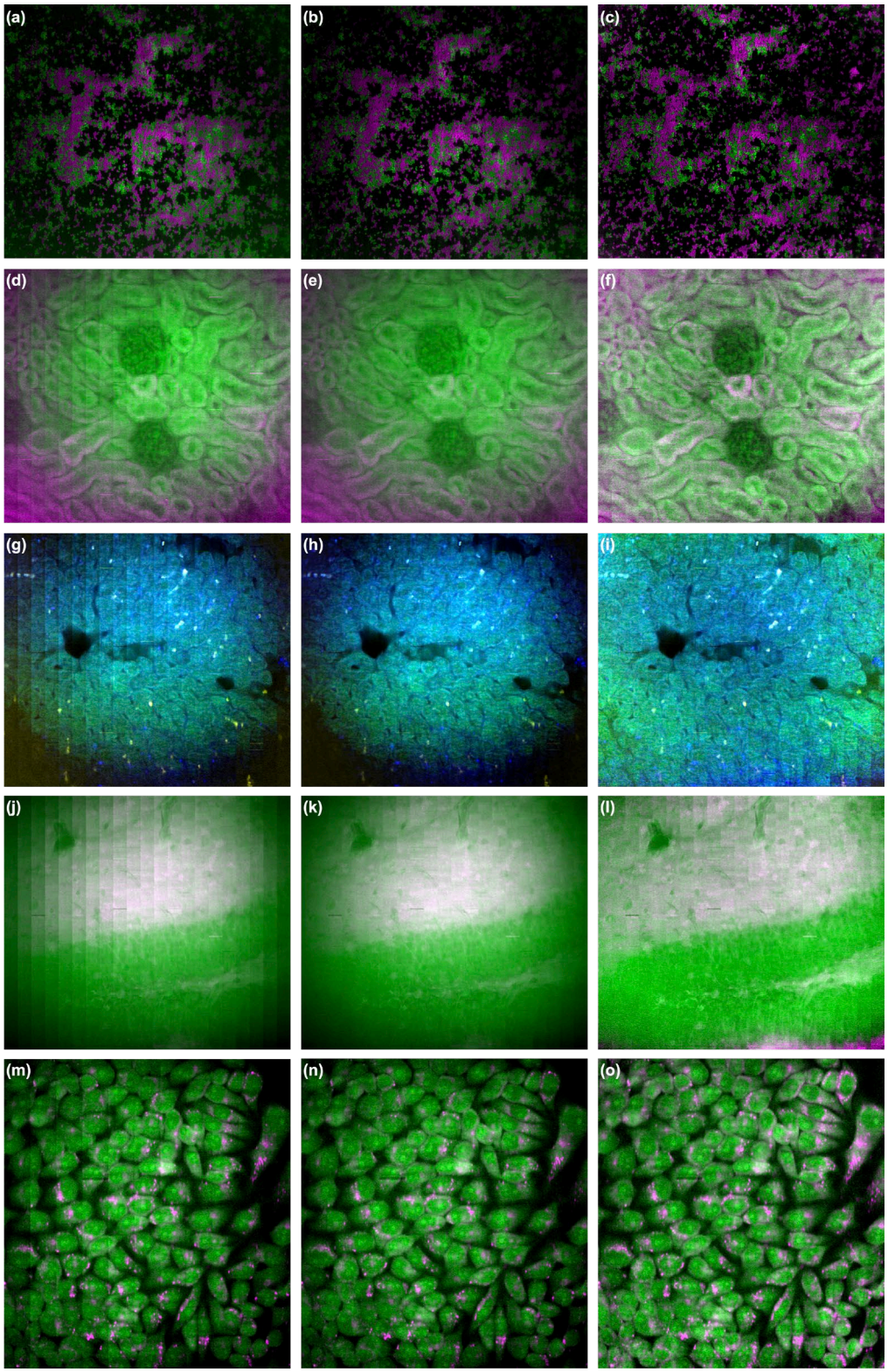
(a)
(b)
(c)
(d)
(e)
(f)
(g)
(h)
(i)
(j)
(k)
(l)
(m)
(n)
(o)

Fig. S2. Multiline illumination Raman images of (a–c) polymer beads, (d–f) kidney tissue, (g–i) liver tissue, (j–l) brain tissue, and (m–o) living cells with neither of stripe and shading corrections (a,d,g,j,m), stripe correction (b,e,h,k,n), and stripe and shading corrections (c,f,i,l,o). Brightness and contrast of the images were adjusted for the visibility of the effects to be clear.